Argon *KLL* Auger spectrum: Initial states, core-hole lifetimes, shake, and knock-down processes

Ralph Püttner [1,*] Philippe Holzhey [1,†] Mateja Hrast,[2] Matjaz Žitnik,[2,3] Gildas Goldsztejn,[4,5] Tatiana Marchenko [4,6]
Renaud Guillemin,[4,6] Loïc Journel,[4,6] Dimitris Koulentianos [7,4,‡] Oksana Travnikova,[4,6] Moustafa Zmerli [4] Denis Céolin,[6]
Yoshiro Azuma,[8] Satoshi Kosugi,[8] Alexandre F. Lago [9] Maria Novella Piancastelli [4,10] and Marc Simon[4,6]

[1]*Fachbereich Physik, Freie Universität Berlin, Arnimallee 14, 14195 Berlin, Germany*
[2]*J. Stefan Institute, Jamova 39, 1000 Ljubljana, Slovenia*
[3]*Faculty of Mathematics and Physics, University of Ljubljana, Jadranska 19, 1000 Ljubljana, Slovenia*
[4]*Sorbonne Université, CNRS, Laboratoire de Chimie Physique-Matière et Rayonnement, 75005 Paris Cedex 05, France*
[5]*Université Paris-Saclay, CNRS, Institut des Sciences Moléculaires d'Orsay, 91405, Orsay, France*
[6]*Synchrotron SOLEIL, L'Orme des Merisiers, Saint-Aubin, 91192 Gif-sur-Yvette Cedex, France*
[7]*Department of Physics, University of Gothenburg, Origovägen 6B, 412 96 Gothenburg, Sweden*
[8]*Department of Materials and Life Sciences, Sophia University, Tokyo 102-8554, Japan*
[9]*Centro de Ciências Naturais e Humanas, Universidade Federal do ABC, 09210-580 Santo André, São Paulo, Brazil*
[10]*Department of Physics and Astronomy, Uppsala University, 75120 Uppsala, Sweden*

State-of-the-art argon *KLL* Auger spectra measured using photon energies of $h\nu = 3216$ and 3400 eV are presented along with an Ar [1*s*] photoelectron spectrum (square brackets indicate holes in the respective orbital). The two different photon energies used for measuring the Auger spectra allow distinguishing between the shake transitions during the Auger decay and the Auger transitions of the photoelectron satellites. A complete assignment of satellite transitions is provided, partially based on configuration-interaction calculations. In addition, Ar $[1s3(s, p)]n'l' \rightarrow [2p^2(^1D_2)]$ transitions are observed, which can be explained by knock-down transitions leading to a direct exchange of angular momentum between the excited electron and the Auger electron. The lifetime broadenings of the Ar [2*s*] single-core-hole state and the $[2s^2]$ and [2*s*2*p*] double-core-hole states are also determined, confirming previously observed trends for double-core-hole states.

I. INTRODUCTION

The *KLL* Auger spectrum of argon was studied extensively in the 1970s and 1980s, both theoretically [1–4] and experimentally [5,6]. In those studies, the dominating diagram lines $[1s] \rightarrow [2s^2(^1S)]$, $[1s] \rightarrow [2s2p(^1P, ^3P)]$, and $[1s] \rightarrow [2p^2(^1S, ^1D, ^3P)]$ were unambiguously assigned; note that throughout this publication square brackets indicate holes in the respective orbital. Moreover, the experimental studies also reported a number of satellite structures. For the *KLL* Auger spectrum of argon such satellites are due to transitions of valence electrons into unoccupied orbitals. These transitions accompany the photoionization as well as the Auger decay and are caused by two different processes, namely, shake and knock. Shake transitions are a consequence of the relaxation process subsequent to ionization which causes a change in the radial wave functions of the orbitals. As a consequence of the ionization process, the orbitals before and after ionization are not orthogonal to each other and the shake transitions can be described by the matrix elements $|\langle nl|n'l', \epsilon'l'\rangle|^2 \neq 0$.

Here *l* indicates the orbital angular momentum, *n* the orbital quantum number, and ϵ a continuum wave function. Moreover, a prime indicates an originally unoccupied orbital in its relaxed form due to ionization and no prime an occupied orbital in the atomic ground state. The matrix element allows only monopole transitions, i.e., $l = l'$, and in the case of Ar 1*s* photoionization only ^2S final states for the ion, e.g., $[1s3p(^{1,3}P)]4p(^2S)$. Note that throughout this publication we omit the prime and double prime (see below) when the principal quantum number *n* is specified (here $n' = 4$).

In a knock process the outgoing electron interacts via Coulomb repulsion with an electron from the valence shell. This allows the exchange of energy and angular momentum between the two electrons and may lead, e.g., in photoionization to the final states $[1s3p(^{1,3}P)]4s(^2P)$. This semiclassical picture is described in a fully quantum mechanical treatment by configuration interaction between the outgoing electron and the electrons remaining in the ion [7]. In the photoionization process one can observe $n' = n$, i.e., the absence of shake which causes the main line as well as $n' > n$, which causes the shake-up or knock-up satellites.

In the case of the Auger decay the shake process can be described with the matrix element $|\langle n'l'|n''l'', \epsilon''l''\rangle|^2$. Here double prime indicates an originally unoccupied orbital in its relaxed form for the case of a double core hole (DCH). As in the case of the photoionization, an additional electron can be promoted to a higher shell ($n'' > n'$) or to the continuum

ϵ, which is called shake-up and/or knock-up and shake-off and/or knock-off, respectively. The Auger process also allows $n'' = n'$, which is in the case of argon for $n' = 3$ a diagram line and for $n' \geqslant 4$ a spectator decay. Finally, in the Auger decay of a photoelectron satellite $n'' < n'$ can be found; this describes a shake-down and/or knock-down process.

Outgoing electrons with high kinetic energy can interact with the valence electrons only within a short time interval leading to a negligible exchange of energy and momentum. These conditions are known as the sudden limit and allow only shake transitions [7]. The fact that different photon energies lead only to small changes in the satellite structure of the photoelectron spectra suggests that for the formation of satellite structures the shake processes are normally dominant over the knock processes [8]. Moreover, for a large number of satellite structures one cannot distinguish between shake and knock based on the given quantum numbers. Because of this, all transitions which are assumed to be predominantly due to the shake process are labeled as such, although knock contributions cannot be excluded. However, some transitions are explicitly assumed to be dominated by the knock process and are therefore labeled in this way. Note that a more detailed recent discussion of the different shake and knock processes has been given by Travnikova *et al.* [9].

We present here a comprehensive assignment of all satellite structures in the *KLL* Auger decay after argon $1s$ photoionization. Despite the complexity of the Auger spectrum, we are able to identify up to six types of different processes (see below for a detailed list).

To perform such a task, both the ionization process and the Auger decay have to be taken into account. In principle, both the ionization and the decay can be accompanied by a shake-up and/or knock-up or a shake-off and/or knock-off process resulting in rich satellite structures. Figure 1 shows the relevant processes for this work, namely, shake-free and/or knock-free or also labeled direct transitions (green solid arrows), shake-up and/or knock-up transitions (blue dash-dotted arrows), shake-down and/or knock-down transitions (red dotted arrows), and shake-off and/or knock-off transitions (magenta dashed arrows); since we measure single-electron emission the latter transitions are not directly visible in the present spectra, but they influence the Auger spectrum by their decay. By taking into account direct as well as shake and knock transitions in both the ionization and the Auger decay, we can distinguish six types of Auger transitions, which are indicated in Fig. 1 by numbers below the down arrows. For convenience, their properties are summarized in the following enumeration.

Type 1: Direct transition in both ionization and decay, i.e., $[1s] \rightarrow [2p^2]$ transitions. These transitions are also known as diagram lines.

Type 2: Direct transition in the ionization process and shake-up during the Auger decay, i.e., $[1s] \rightarrow [2p^23l]n''l''$.

Type 3: Shake-up during the ionization process and shake-down and/ or knock-down during the Auger decay, i.e., $[1s3l]nl' \rightarrow [2p^2]$. We will show below that this type of Auger transition is mostly due to the knock mechanism.

Type 4: Shake-up during the ionization process and direct transition during Auger decay, i.e., $[1s3l]n'l' \rightarrow [2p^23l]n''l''$,
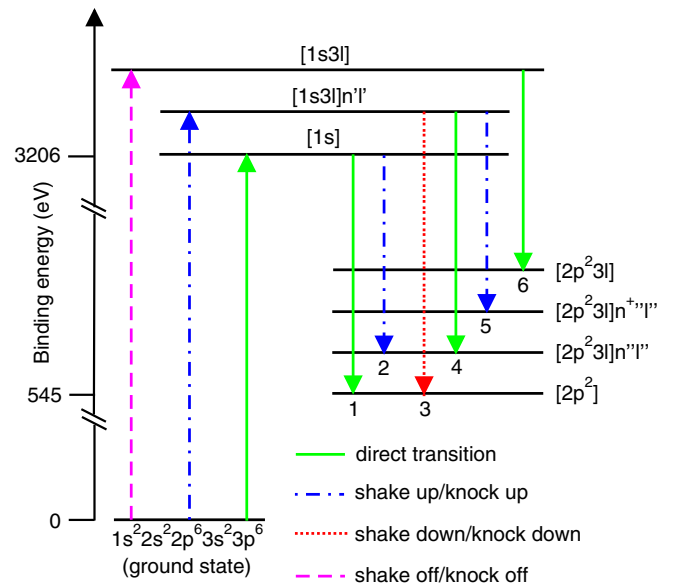

FIG. 1. Schematic picture of the ionization and the decay processes contributing to the *KLL* Auger spectrum of argon. The green solid lines indicate shake-free and/or knock-free direct transitions, while the blue dash-dotted lines and red dotted lines represent shake-up and/or knock-up and shake-down and/or knock-down processes, respectively. The dashed magenta line indicates a double-ionization process based on the shake-off and/or knock-off mechanism which is not observed directly but contributes to the Auger spectrum. Note that $n^+ > n$, i.e., $n'l' \rightarrow n^{+''}l''$ describes a shake-up and/or knock-up process (type 5). The different types of Auger processes are labeled by numbers below the down arrows. For details, see the text.

with $n' = n''$ and $l' = l''$. These transitions are also known as spectator Auger decay.

Type 5: Shake-up during both ionization and decay, i.e., $[1s3l]n'l' \rightarrow [2p^23l]n^{+''}l''$, with $n^+ > n$.

Type 6: Shake-off during ionization and direct transition during Auger decay, i.e., $[1s3l] \rightarrow [2p^23l]$.

Despite the fact that all processes are possible, in Refs. [5,6] the satellites were discussed only in terms of Auger decays of the shake-up (type 4) or shake-off (type 6) satellites of the photoionization process. In the cited publications [5,6] the valence-shell photoionization satellites, i.e., $[1s3(s, p)]n'l', \epsilon'l'$ states, and core-level photoionization satellites, i.e., $[1s2(s, p)]n'l'$ states, were taken into account as initial states of the Auger decay. However, during the decay only two-electron direct Auger transitions (green solid down arrows of types 1, 4, and 6) were considered, i.e., shake processes during the Auger decay (types 2, 3, and 5) were neglected in the assignment of the spectral features. Moreover, Schmidt stated [10] that shake processes during the Auger decay were not observed at that time. For the molecules isoelectronic to argon, namely, HCl, H_2S, PH_3, and SiH_4, similar assignments of the different structures visible in the *KLL* Auger spectra are given (see Refs. [5,11,12]).

In resonant *KLL* spectra, shake transitions in the valence shell during Auger decay (type 5) are actually common [13–17], since the excited species possess an open-shell structure. Nevertheless, they are widely neglected in the analysis of normal Auger spectra and were found only for the open-shell

atoms sodium [18] and silicon [19] as well as by some of the present authors for the closed-shell molecule H_2S [20]. In addition, this study on H_2S showed Auger decays of the S $[1s\,V]n'l'$ (V denotes the valence orbital) shake-up states of photoionization process. Auger decays of the $[1s2(s, p)]n'l'$ core level shake-up states were not clearly identified, although they were used in earlier publications for the assignment of the satellites in the *KLL* Auger spectrum of H_2S [11,12] and argon [6]. In Ref. [20] the different processes were identified by the photon energy used for the photoionization process; such a procedure became possible in recent years due to significant improvement in instrumentation for hard-x-ray photoelectron spectroscopy (HAXPES) also available for gas-phase measurements [21]. In more detail, a shake process during the Auger decay (type 2) is possible at all photon energies above the $[1s]$ ionization energy. Contrary to this, Auger decays of the $[1s\,V]n'l'$ and $[1s2(s, p)]n'l'$ shake states (types 4–6) are possible only with photon energies that are high enough to form the corresponding initial state, i.e., $h\nu > E_{bin}(1s) + E_{exc}(3l \rightarrow n'l')$ with $E_{bin}(1s)$ being the Ar $1s$ binding energy and $E_{exc}(3l \rightarrow n'l')$ the excitation energy for a $3l$ electron into the $n'l'$ level.

The present study of the *KLL* Auger spectrum of argon is performed by using the same approach as in Ref. [20], i.e., by using different ionization energies, and finds likewise shake processes during the Auger decay (type 2) as well as Auger decays of $[1s3(s, p)]n'l'$ satellite states in the photoionization process (types 4–6). These results are fully confirmed by complementary calculations. For a better understanding of the Auger decays of $[1s3(s, p)]n'l'$ satellites, we also present and discuss the satellites in the Ar $[1s]$ photoelectron spectrum.

Although the present results are similar to those observed for H_2S [20], the spectral structure of argon is however simpler than that of H_2S, due to the absence of the nuclear degrees of freedom, so the electronic structure could be identified in deeper detail. In particular, in this way we obtain access to the highly excited DCH states of the configurations $[2p^23p]n''(p'', d'')$ and observe the splitting of the $[2p^2(^1D)3p]$ configuration into the components $(^2P, ^2D, ^2F)$ due to the coupling of the $[3p]$ hole to the $[2p^2(^1D)]$ holes. In addition, $[1s3(s, p)]n'(s', p') \rightarrow [2p^2(^1D)]$ transitions are observed, which are predominantly due to knock-down processes (type 3). Moreover, the three components of the total angular momentum J to the final states $^3P_2$, $^3P_1$, and $^3P_0$ of the $[1s] \rightarrow [2s2p(^3P)]$ diagram lines are resolved and for all diagram lines accurate energies are reported. Finally, lifetime broadenings of the $[2s]$ single-core-hole (SCH) state and the $[2s^2]$ as well $[2s2p]$ DCH states are given, confirming recent results which demonstrated that the lifetime broadenings of DCH states are not just given by the sum of those of the involved SCH states [22–24].

II. EXPERIMENTAL SETUP AND CALCULATIONAL DETAILS

The measurements were performed at the SOLEIL synchrotron, France, on the GALAXIES beamline, with an endstation dedicated to HAXPES [21,25]. Linearly polarized light was provided by a U20 undulator and energy selected by a Si(111) double-crystal monochromator. Photoelectron spec-

tra were collected with a SCIENTA EW4000 hemispherical electron analyzer specifically designed for HAXPES.

The $KL_{2,3}L_{2,3}$ Auger spectra relevant for the present study were measured using the photon energies $h\nu = 3216$ and 3400 eV in order to discriminate different processes like Auger transitions of the photoelectron satellites and shake transitions during the Auger decay (for details see below). Moreover, a *KLL* overview spectrum including final states with L_1 holes has been measured at a photon energy of 4500 eV. For these measurements an analyzer pass energy of $E_{pass} = 200$ eV and a slit width of 500 μm were applied, resulting in a spectrometer resolution of $\cong 550$ meV. The Ar $[1s]$ photoelectron spectrum was recorded using the same parameter settings for the electron analyzer. However, the additional photon bandwidth at the used photon energy $h\nu = 3900$ eV leads to a larger total resolution of $\cong 700$ meV. For the Ar $[2s]$ photoelectron spectrum a photon energy of 2400 eV, a slit width of 300 μm, and a pass energy of $E_{pass} = 200$ eV were used, giving a Gaussian resolution of 545(10) meV.

The Ar $[1s]$ photoelectron spectrum was calibrated to the value of $E_{bin} = 3206.3(3)$ eV for the binding energy [26], while for the Auger spectra a kinetic energy of 2660.51(1) eV for the $[1s] \rightarrow [2p^2(^1D_2)]$ transition was used [6]. The Ar $[2s]$ photoelectron spectrum was calibrated using a small N_2 impurity with binding energies for the N $[1s_g]$ and N $[1s_u]$ core-hole states of 409.93(1) and 409.82(1) eV, respectively [27].

The theoretical approach based on configuration interaction reproduced recently the measured Ar *KLL* spectrum [22]. The same semirelativistic approach is employed below to estimate a spectral contribution of the shake-up Auger *KM-LLM* decay. In parallel, a fully relativistic multiconfiguration Dirac-Fock calculation of Auger amplitude between relaxed initial and final states was executed [28,29], as described in detail in a recent study performed by some of the present authors [30]. In both cases the results are compared to experimental data using final states described by a mixture of $[2p^23p](3d, 4s, 4p, 4d, 5p, 6p)$ configurations.

III. THE Ar $[1s]$ PHOTOELECTRON SPECTRUM

We first discuss the Ar $[1s]$ photoelectron spectrum including the shake-up structures originating from valence orbitals, as such shake processes are relevant for about 20% of the transitions and produce additional initial states for the Auger decay [31–33]. The valence shake transitions of Ar have been investigated theoretically by Dyall [31] and experimentally by Southworth *et al.* [8]. Their work focused on the single-shake-up transitions to the $[1s3p]n'p'$ and $[1s3s]n's'$ final states and demonstrated that the calculations of Dyall [31] describe the single-shake-up region in terms of energy positions and intensities very well. We present in Fig. 2 a spectrum with improved signal-to-noise ratio and high resolution showing also double-shake-up transitions of the type $[1s3p^2]n_1'l_1'n_2'l_2'$; note that the lower indices 1 and 2 describe the two excited electrons. The spectrum can be divided in three regions, namely, the Ar $[1s]$ main line located at a binding energy of 3206.3(3) eV as well as the single-shake-up region at relative binding energies of 20–48 eV and the double-shake-up region with relative binding energies above the latter value.
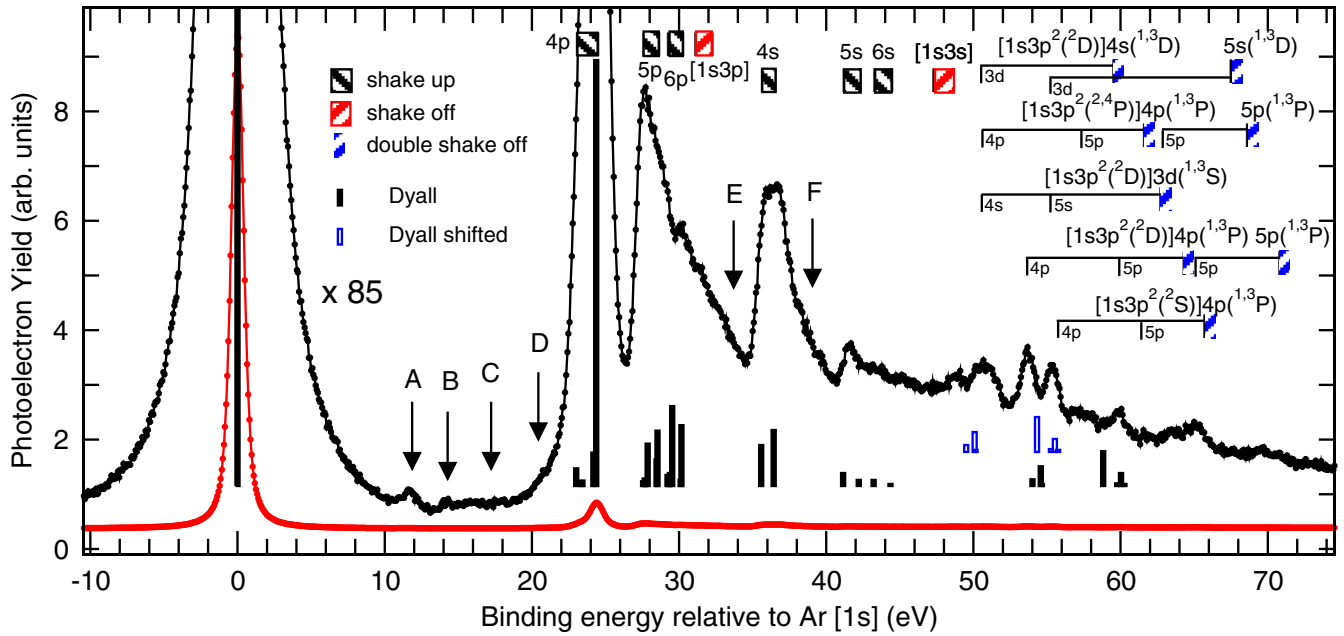
FIG. 2. The Ar [1*s*] photoelectron spectrum including the region of the valence orbital shake-up structures (relative binding energies of 20–48 eV) and double-shake-up structures (above 48 eV) measured using a photon energy of $h\nu = 3900$ eV. For the black line the intensity axis is stretched by a factor of 85. The vertical bars indicate the energy positions and intensities as calculated by Dyall [31]. The assignments of the single-shake-up states are indicated by boxes that show the spread of the states belonging to a given configuration. The red boxes filled diagonally from bottom left to top right and labeled by [1*s*3*p*] and [1*s*3*s*] indicate the double-ionization thresholds populated via shake-off. The black boxes filled diagonally from top left to bottom right labeled $n's'$ or $n'p'$ indicate the corresponding single-shake-up states. The spectral features labeled A to F are discussed in the text. In the double-shake-up region above 48 eV the estimated positions for the double-shake-up states and the corresponding ionization thresholds are indicated by the vertical bar diagrams above the spectrum. The labels above the horizontal lines of the type $[1s3p^2(^SL)]n'l'(^{S'}L')$ specify the double-ionization thresholds, which are represented with diagonal blue lines from bottom left to up right. The labels next to the small vertical lines of the type $n'l'$ specify the second excited electron. The hollow blue bars below the spectrum indicate the theoretical predictions of Dyall for the double-shake transitions, however, shifted to lower energies by 4.5 eV.

The calculations of Dyall [31] (black vertical bars in Fig. 2) take only direct shake transitions into account. In these transitions the 1*s* electron interacts with the photon and is promoted into the continuum while a 3*s* or 3*p* electron is excited via shake into a $n's'$ or $n'p'$ orbital. These direct shake transitions are described by the matrix element $|\langle nl|n'l'\rangle|^2$. As mentioned above, only monopole transitions, i.e., $l = l'$, are allowed based on the matrix element. Moreover, this matrix element leads only to a ^2S symmetry for the final ionic state, which is strictly valid in pure *LS* coupling. However, Dyall took also relativistic effects into account, which lead to a configuration mixing and weak spectral contributions caused by final ionic states with symmetries different from ^2S. These final ionic states are important in the discussion of the knock-down Auger decays (type 3) (discussed below).

The assignment for the single-shake transition resulting from the work of Dyall [31] is indicated in the upper part of the spectrum by boxes filled with diagonal lines. The energy positions for the [1*s*3*s*] and [1*s*3*p*] thresholds are estimated by using the $Z + 1$ approximation, i.e., the ionization thresholds of K II [34], as well as the theoretical spin-orbit and exchange splittings for corresponding thresholds in argon [31]. In addition to the calculated shake satellites, the spectrum shows six small spectral features indicated with A–F, which are not reproduced by the theoretical work of Dyall [31]. Structures A–D are previously explained in Ref. [8]. In detail, structures A–C originate from energy losses of the Ar [1*s*] photoelec-

tron that lead to interatomic processes, namely, $3p \rightarrow 4s$, $3p \rightarrow 5s$, and $3p \rightarrow ns$ transitions, with $n \geqslant 6$ in a neutral argon atom. Based on calculations, Southworth *et al.* assigned shoulder D to [1*s*3*p*]3*d* and [1*s*3*p*]4*s* shake transitions [8].

A second type of shake process is the conjugate shake process. In this case the photon promotes the 1*s* electron in an $n'p'$ orbital, accompanied by a monopole shake of a 3*s* or 3*p* electron into the $\epsilon s, p$ continuum. Shoulder F is assigned as such a transition. It is located at the high-energy side of the [1*s*3*s*]4*s* transitions and possesses a binding energy which is 39 eV higher than that of the [1*s*] level. In detail, we assign it to the [1*s*3*s*]4*p* conjugate shake transitions since its term value of $\cong 9$ eV relative to the [1*s*3*s*] threshold agrees well with the term value of $\cong 8$ eV for the [1*s*3*p*]4*p* shake transitions relative to the [1*s*3*p*] threshold.

The energy region indicated by E is between the exchange and spin-orbit split $[1s3p(^1P, {}^3P_{2,1,0})]$ thresholds and the lowest [1*s*3*s*]4*s* transitions, so the strong decrease of the photoionization cross section cannot be explained by single-shake-up states. A similar spectral feature is observed for the shake region of neon and explained by the shake-off continuum [35,36], i.e., by a double ionization with the emission of a fast photoelectron and a very slow shake-off electron. We assume that this is also valid for argon.

As shown in Fig. 2, the most relevant excited initial states for the *KLL* Auger spectrum are the singly ionized states [1*s*3*p*]4*p* and [1*s*3*p*]5*p*, as well as the doubly ionized states

[1s3p]. The latter are due to shake-off transitions and are shown to represent $\cong 20\%$ of the intensity of the [1s] main line [32,33].

In the double-shake-up region above 48 eV relative binding energy there is no obvious agreement with the predictions by Dyall [31]. In order to obtain an approach to the assignment we indicated with the diagonal blue lines from the bottom left to the top right the expected energy positions for a number of double-ionization thresholds. Above the corresponding horizontal lines the thresholds are labeled by $[1s3p^2]n'l'(^{S'}L')$. The labels next to the small vertical lines of the type $n'l'$ specify the second excited electron.

The thresholds $[1s3p^2(^2D)]4s, 5s(^{1,3}D)$, $[1s3p^2(^2D)]3d(^{1,3}S)$, and $[1s3p^2(^4P)]4p$ are estimated based on the $Z+1$ approximation, i.e., we assume that their binding energy relative to the [1s] line is identical to the respective states in K III relative to the ground state of K II; the corresponding energy values are taken from NIST [34]. The remaining thresholds are estimated based on the thresholds obtained from the $Z+1$ approximation and the theoretical splittings between the $[1s3p^2]n'l'$ obtained by Dyall [31].

Using the indicated thresholds, the different $[1s3p^2]4p^2$ satellites calculated by Dyall [31] possess term values of $\cong 8$ eV, i.e., comparable to the values for the $[1s3p]4p$ satellites. However, it should be expected that a $4p$ electron screens another $4p$ electron less from the atomic core than a $3p$ electron. Consequently, we expect larger $4p$ term values for the $[1s3p^2]4p^2$ configuration than for the $[1s3p]4p$ configuration. From this we conclude that the calculated energy positions for the double-shake-up states are too high in energy.

By shifting the calculated values for the double-shake satellites by 4.5 eV towards lower energies (hollow vertical bars), a reasonable agreement with the spectral features is reached. Based on this finding, we tentatively assign the broad peak at $\cong 51$ eV relative binding energy to the $[1s3p^2(^2D)]4s(^1D)3d(^2S_{1/2})$, $[1s3p^2(^2D)]4s(^3D)3d(^2S_{1/2})$, and $[1s3p^2(^4P)]4p^2(^1D)(^4P_{1/2})$ satellites, the peak at $\cong 53.5$ eV to $[1s3p^2(^2D)]4p^2(^1D)(^2S_{1/2})$ satellite, and the peak at $\cong 55.5$ eV to the $[1s3p^2(^2D)]5s(^1D)3d(^2S_{1/2})$, $[1s3p^2(^2D)]5s(^3D)3d(^2S_{1/2})$, and $[1s3p^2(^2S)]4p^2(^1S)(^2S_{1/2})$ satellites. The respective assignments are indicated by small vertical bars in the upper part of the figure. Based on this assignment as well as the indicated thresholds, we assigned the remaining spectral features to $[1s3p^2]4p5p$ and $[1s3p^2]5p^2$ double-shake satellites; see also small vertical bars above the spectrum.

IV. THE Ar *KLL* AUGER DECAY

Figure 3 shows the overview spectrum of the *KLL* Auger transitions measured using a photon energy of $h\nu = 4500$ eV, i.e., the spectrum contains all possible shake processes. In this figure the different diagram lines (type 1) are indicated by vertical-bar diagrams above the spectrum. All lines not indicated represent the shake structures which are the main target of the present investigation. For this study we restrict the spectrum to the Auger energy range from 2605 to 2655 eV with the $[1s] \rightarrow [2p^2]$ Auger transitions (see Fig. 4) for two different reasons. First, previous studies on H$_2$S [20] showed that each diagram line possesses the same shake structure.
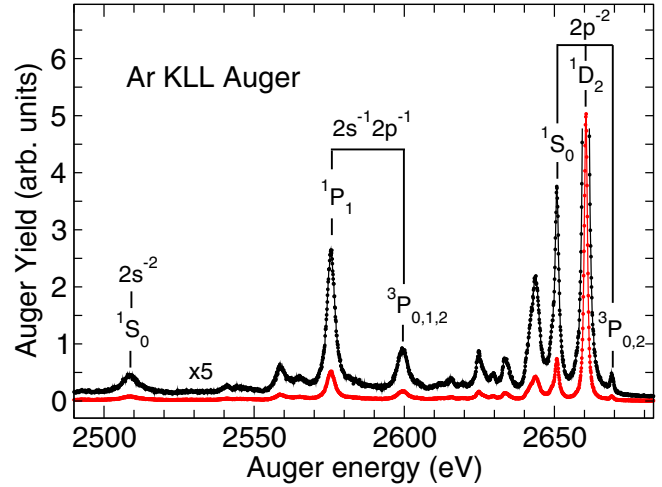

FIG. 3. The *KLL* Auger spectra measured subsequent to photoionization with a photon energy of $h\nu = 4500$ eV. The diagram lines are indicated by the vertical-bar diagrams above the spectrum while all other spectral features are due to shake structures.

Second, the linewidths of the $[1s] \rightarrow [2s^2]$ and the $[1s] \rightarrow [2s2p]$ Auger transitions are larger due to the shorter lifetime of the 2s hole, so the strongly overlapping shake transitions cannot be resolved.

Based on the Ar [1s] photoelectron spectrum previously discussed, we selected two different photon energies, namely, $h\nu = 3216$ and 3400 eV, for the ionization process of the *KLL* Auger spectra used in the data analysis. The photon energy $h\nu = 3216$ eV was selected in order to exclude contributions from the Auger decays of shake-up structures in the
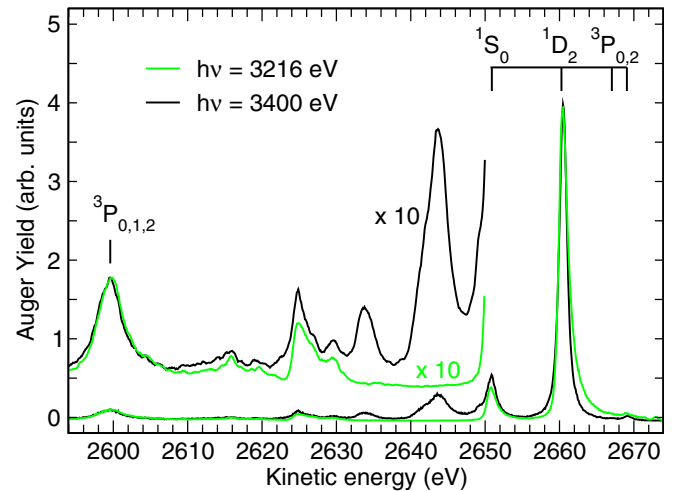

FIG. 4. The *KLL* Auger spectra in the region of the $[1s] \rightarrow [2p^2(^1S_0, ^1D_2, ^3P_{0,2})]$ transitions and the $[1s] \rightarrow [2s2p(^3P_{0,1,2})]$ diagram lines measured subsequent to photoionization with a photon energy of $h\nu = 3216$ eV (green) and $h\nu = 3400$ eV (black). The diagram lines are indicated by vertical bars above the spectra. For reasons of presentation, the green spectrum measured at $h\nu = 3216$ eV is shifted by 0.55 eV to lower energies to compensate for the PCI shift. For the same reasons, the spectra multiplied by 10 are smoothed by averaging over five neighboring points.

photoelectron spectrum (types 4–6), while at $h\nu = 3400$ eV the shake-up contributions are expected to be fully developed. The spectra measured with photon energies of $h\nu = 3216$ and 3400 eV are presented in Fig. 4 in green and black, respectively, and show remarkable differences. The energy positions of the Ar $[1s] \rightarrow [2p^2(^1S_0, {}^1D_2, {}^3P_{0,2})]$ and Ar $[1s] \rightarrow [2s2p(^3P_{0,1,2})]$ diagram lines are indicated by the vertical bars above the spectrum. In the case of the spectrum measured at an ionization energy of $h\nu = 3216$ eV only the Ar $[1s]$ state can be populated, so all lines but the diagram in this spectrum are due to shake processes during the Auger decay (type 2).

The spectrum measured subsequent to a photoionization energy of $h\nu = 3400$ eV shows additional significant spectral features, mainly in the kinetic energy region from 2630 to 2650 eV, which are assigned to the Auger spectra of the satellite states observable in the photoelectron spectrum, i.e., types 4–6.

For reasons of presentation, the green spectrum measured at $h\nu = 3216$ eV is shifted by 0.55 eV to lower energies to compensate for the postcollision interaction (PCI) shift. Moreover, the Ar $[1s] \rightarrow [2p^2(^1S_0, {}^1D_2)]$ transitions show a significant PCI distortion. In contrast to this, such a modification of the line shape is practically absent for the Ar $[1s] \rightarrow [2s2p(^3P_{0,1,2})]$ lines measured at the same photon energy. These differences are explained by the fact that the line shapes are formed by PCI line shapes with a width of 655 meV [21] due to the Ar $[1s]$ lifetime, convoluted with a Lorentzian of the lifetime widths of the final states [37]. This final-state lifetime width amounts for the $[2p^2]$ states to 323(15) meV [22] and for the $[2s2p]$ states to 2.17(2) eV (discussed below); the convolution with a Lorentzian of the latter value masks the PCI distortion almost completely. The influence of postcollision interaction for argon is discussed in detail in [37,38].

In the following we will first discuss in Sec. IV A the shake-up processes during the Auger decay (type 2), based on the spectrum measured at $h\nu = 3216$ eV. Then we will discuss in Sec. IV B the Auger decays of the shake-up lines in the photoelectron spectrum which are only present in the spectrum recorded using a photon energy of $h\nu = 3400$ eV, namely, types 4–6. Moreover, we present in Sec. IV C the Ar $[1s] \rightarrow [2s2p(^3P)]$ diagram line including the splitting into the final states $(^3P_{2,1,0})$. Finally, the Ar $[2s]$ photoelectron and the Ar $[1s] \rightarrow [2s^2]$ and Ar $[1s] \rightarrow [2s2p]$ transitions are fitted in order to determine the lifetime broadenings of the Ar $[2s]$ single core hole and the Ar $[2s^2]$ and $[2s2p]$ double core holes (Sec. IV D).

A. The Ar $[1s] \rightarrow [2p^2(^1S_0, {}^1D_2, {}^3P_{0,2})]3p]n''(p'', d'')$ Auger shake-up transitions

In this section we discuss the shake transitions during the Auger decay (type 2). For this purpose Fig. 5 shows the corresponding *KLL* Auger spectrum measured subsequent to a photon energy of $h\nu = 3216$ eV together with two different calculations, which are used to support the assignment of the shake-up transitions. The relativistic calculations shown in Fig. 5(b) are performed by including different configurations. The black, red, and blue spectra show the results by including only the $[2p^23p]4p$ configuration, the configurations
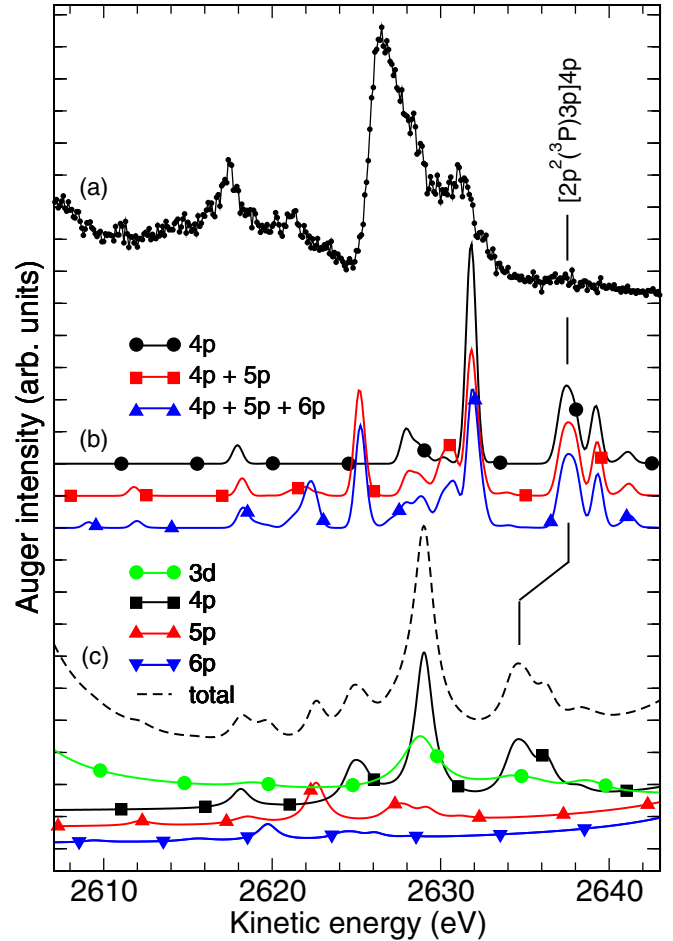

FIG. 5. Region of the Ar $[1s] \rightarrow [2p^2(^1S_0, {}^1D_2, {}^3P_{0,2})3p]n(p, d)$ Auger shake-up transitions. (a) Experimental results. (b) Relativistic calculations. The black line with circles shows the calculations including only the $[2p^23p]4p$ configuration. The red (blue) line with squares (up triangles) displays the results of the calculations taking the configurations $[2p^23p]4p$ and $[2p^23p]5p$ ($[2p^23p]4p$, $[2p^23p]5p$, and $[2p^23p]6p$) into account. (c) Nonrelativistic calculations. Shown are the contributions of the configurations $[2p^23p]3d$ (green solid line with circles), $[2p^23p]4p$ (black solid line with squares), $[2p^23p]5p$ (red solid line with up triangles), and $[2p^23p]6p$ (blue solid line with down triangles) as well as the total spectrum (black dashed line). Note that the baselines of the contributions in (b) and (c) are shifted relative to each other.

$[2p^23p]4p$ and $[2p^23p]5p$, and the configurations $[2p^23p]4p$, $[2p^23p]5p$, and $[2p^23p]6p$, respectively. The nonrelativistic calculations shown in Fig. 5(c) include the configurations $[2p^23p]3d$ (green solid line), $[2p^23p]4p$ (black solid line), $[2p^23p]5p$ (red solid line), and $[2p^23p]6p$ (blue solid line), as well as $[2p^23p]4s$ and $[2p^23p]4d$. The latter two configurations show only minor contributions and are not shown in Fig. 5(c) for clarity.

Both calculations show differences in the absolute intensities and energy positions and resemble only qualitatively the experimental Auger spectrum. This prevents a detailed assignment of the shake structures based on the calculations. However, they suggest that the configurations $[2p^23p]3d$,

$[2p^23p]4p$, $[2p^23p]5p$, and $[2p^23p]6p$ have to be taken into account.

In order to achieve an approach to the assignment of the observed transitions, a combined approach consisting of a fit analysis, the two calculations, and the $Z + 2$ model is utilized. In the following we first describe our fit model and the result of the fit analysis. After this we assign the observed spectral features using our calculations and the $Z + 2$ model.

In the fit approach, only transitions to the $[2p^2(^1S_0, {}^1D_2)3p]n''(p'', d'')$ final states were taken into account. The transitions to the $[2p^2(^3P_{0,2})3p]n''(p'', d'')$ states were neglected since even the most intense ones of this type, namely, the $[2p^2(^3P_{0,2})3p]4p$ [see Fig. 5(a)], are hardly visible in the experimental results. In a first fit approach identical energy splittings between the Ar $[1s] \to [2p^2(^1S_0, {}^1D_2)]$ diagram lines and the Ar $[1s] \to [2p^2(^1S_0, {}^1D_2)3p]n''(p'', d'')$ shake transitions were assumed, i.e., a coupling of the $3p$ electron to the $[2p^2(^1S_0, {}^1D_2)]$ states was neglected. Since this approach did not result in a satisfactory description of the spectrum, in the next step coupling between the $[2p^2]$ double core hole and the $[3p]$ valence hole was included. In this way we arrived at the states $[2p^2(^1S_0)3p(^2P)]$ and $[2p^2(^1D_0)3p(^2P, {}^2D, {}^2F)]$, i.e., fourfold splitting. For the shake transitions spin flips were assumed to be very small, so quartet states were neglected. The spin-orbit interactions of the ^2L states with the components $J = L + 1/2$ and $J = L - 1/2$ were also neglected since the resulting splittings were calculated to be on the order of 0.2–0.5 eV, depending on the individual states $[2p^2(^1S_0)3p(^2P)]$ and $[2p^2(^1D_2)3p(^2P, {}^2D, {}^2F)]$. Note that these splittings agree well with the spin-orbit splitting of the $3p^{-1}$ state in the $Z + 2$ atom Ca IV of $\cong 385$ meV [34]. These splittings are significantly smaller than the lifetime broadening $\Gamma = \Gamma_{[1s]} + \Gamma_{[2p^2]} = 655$ meV $+ 323$ meV $= 978$ meV [21,22], justifying an omission. As for lifetime broadenings, the same values as for the main lines were applied.

Figure 6 shows the fit result of the Auger spectrum in the region of the shake transitions which go along with the $[1s] \to [2p^2(^1S_0, {}^1D_2)]$ diagram line; the corresponding spectrum is recorded using a photon energy of $h\nu = 3216$ eV. The red solid line through the data points represents the fit result and the black dashed line the background.

In detail, the background consists of a step at $\cong 2615$ eV, as well as two broad Gaussians at $\cong 2637$ eV and at $\cong 2645$ eV. The step at $\cong 2615$ eV takes into account the $[1s] \to [2p^2(^1D_2)3p]\epsilon l$ shake-off transitions. The first broad Gaussian at $\cong 2637$ eV is assigned to the weak $[1s] \to [2p^2(^3P_{2,0})3p]4p$ transitions. This assignment is based on the present calculations (see Fig. 5), which predict such transitions in this energy range, however, with strongly overestimated intensities. The second broad Gaussian at $\cong 2645$ eV is, based on energy arguments, preliminarily assigned to a recapture process of the type $[1s]\epsilon p \to [2p^2(^1D_2)3p]4p^2$, i.e., a recapture of the photoelectron during the Auger decay. This preliminary assignment is based on energy arguments since at the used photon energy of $h\nu = 3216$ eV the energy position of the $[1s]\epsilon p \to [2p^2(^1D_2)]4p$ transition is found $\cong 19$ eV above the $[1s] \to [2p^2(^1D_2)]$ diagram line [37]. The same splitting is observed between the $[1s] \to [2p^2(^3P_{2,0})3p]4p$
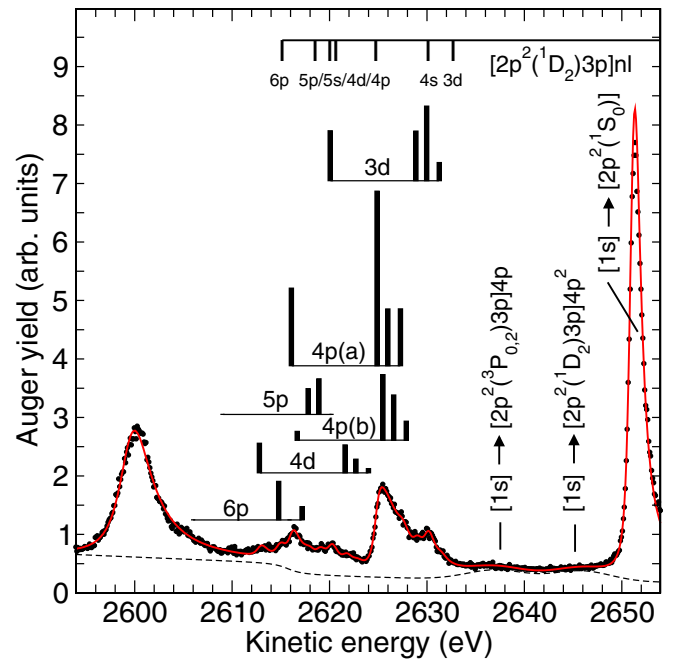

FIG. 6. Fit result of the Ar $[1s] \to [2p^2(^1S_0, {}^1D_2)]$ Auger spectrum in the region of the shake transitions; this spectrum is recorded with a photon energy $h\nu = 3216$ eV. The red solid line through the data points represents the fit result and the black dashed line the background. The six vertical-bar diagrams indicate the energy positions and relative intensities of the observed shake-up Auger transitions. The vertical-bar diagram in the upper part of the spectrum indicates the energy positions of the $[1s] \to [2p^2(^1D_2)3p]n''l''$ shake-up transitions using the $Z + 2$ approximation as well as the energy position of the $[1s] \to [2p^2(^1D_2)]$ diagram line as a reference.

transitions observed at 2626 eV (discussed below) and the discussed broad Gaussian feature at 2645 eV. At $\cong 2651$ eV the intense $[1s] \to [2p^2(^1S_0)]$ diagram line can be seen.

The six vertical-bar diagrams shown in Fig. 6 indicate the main results of the fit analysis, namely, the energy positions and intensities of the shake-up transitions during the Auger decay. From the fit analysis we obtained splittings of 8.7(1), 9.9(1), and 11.7(3) eV between the transitions to final states with the parent states $[2p^2(^1S_0)3p(^2P)]$ and $[2p^2(^1D_2)3p(^2P, {}^2D, {}^2F)]$. These values agree well with the results of the present relativistic calculations of 8.5, 10.0, and 13.2 eV and indicate that the applied fit approach describes the essential parts of the physics involved. From the fit analysis we also derive that the intensity of the shakes during the Auger decay amounts 4.8(1.0)% of the total Auger intensity. This value is based on the assumption that the shake probability is independent of the $[2(s, p)^2]$ final state.

In the next step we assign the shake transitions. The six vertical-bar diagrams show that not only monopole shake transitions (i.e., $3p \to n''p''$ transitions where both electrons couple to ^1S) contribute to the spectrum since only three of such transitions ($n = 4, 5, 6$) are expected in this energy region. To assign the observed transitions we utilize the above-given calculation which suggests that the configurations $[2p^23p]3d$, $[2p^23p]4p$, $[2p^23p]5p$, and $[2p^23p]6p$ have

to be taken into account. As mentioned above, we employ the $Z + 2$ approximation, i.e., the energy values of excitations in Ca III [34], to estimate the energy positions of the final states $[2p^2(^1D_2)3p]n''l''$; these values are given by the vertical-bar diagram in the upper part of the figure. Based on these data, we assign the obtained final-state configuration to $[2p^23p]3d$, $[2p^23p]4p$, $[2p^23p]4d$, $[2p^23p]5p$, and $[2p^23p]6p$ as indicated in Fig. 6. The two multiplets labeled $4p(a)$ and $4p(b)$ are split by $\cong 750$ meV and are both assigned to the $[2p^23p]4p$ due to the small splitting and the large intensity.

The suggested additional splitting of $[2p^23p]4p$ configuration can be understood by assuming monopole shake transitions. In this case the $3p$ hole and the $4p$ electron couple to ^1S. As a result, the final states have to have either ^1S or ^1D symmetry, based on the coupling of the two $2p$ holes. By taking the spin-orbit interaction due to the $3p$ hole into account, one obtains in *LS* coupling the final states $[2p^2(^1S_0)3p(^2P_{1/2,3/2})]4p(^1S_0)$ and $[2p^2(^1D_2)3p(^2P_{1/2,3/2}, {}^2D_{3/2,5/2}, {}^2F_{5/2,7/2})]4p(^1D_2)$, i.e., two final states belonging to $[2p^2(^1S_0)]$ and six final states belonging to $[2p^2(^1D_2)]$. Generally, only half of these states are observed, since spin-orbit interaction is too low to be resolved (discussed above). However, due to the spatial vicinity of the $3p$ hole and the $4p$ electron, the interaction is expected to be stronger than for a higher-n'' $[2p^23p]n''p''$ configuration. This can lead to a splitting between, e.g., the $[2p^2(^1D_2)3p(^2P_{1/2,3/2})]4p(^1D_2)$ states, which is larger than the spin-orbit splitting between the $[2p^2(^1D_2)3p(^2P_{1/2,3/2})]$ parent states and can explain the observed splitting. For higher n'' the described effect is too small and only the splittings of the parent states are observable.

As already mentioned above, the given assignment including the final-state configurations $[2p^23p]3d$ and $[2p^23p]4d$ demonstrates that also nonmonopole shake transitions contribute to the spectrum. As a consequence, other nonmonopole transitions like Ar $[1s] \rightarrow [2p^23p]n''p''$ with $3p$ and $n''p''$ coupling to a symmetry different from ^1S cannot be excluded. As for the photoelectron spectrum (discussed above), such nonmonopole shake transitions can be explained by configuration interaction of the ionic states caused by relativistic effects. Finally, we want to point out that in the present fit analysis we observe a large number of overlapping lines, so the intensity information given by the vertical bars is not very reliable. In particular, the energy positions of the transitions $[1s] \rightarrow [2p^2(^1S_0)3p(^2P)]3d$ and $[1s] \rightarrow [2p^2(^1D_2)3p(^2F)]5p$ overlap strongly in our fit analysis. Based on this analysis, the spectral intensity is assigned to the first transition, although in reality it is probably shared by both transitions. In summary, we give a coherent assignment based on calculations and the $Z + 2$ approximation. However, for an ultimate assignment much more sophisticated calculations have to be performed.

B. Auger decays of Ar $[1s3(s, p)]n'l'$ shake-up and $[1s3(s, p)]$ shake-off states

In this section we focus on the Auger decays of the Ar $[1s3(s, p)]n'l'$ shake-up and $[1s3(s, p)]$ shake-off states. In the first step we discuss the region of the shake-up and spectator decays during the Auger process (types 4–6), which
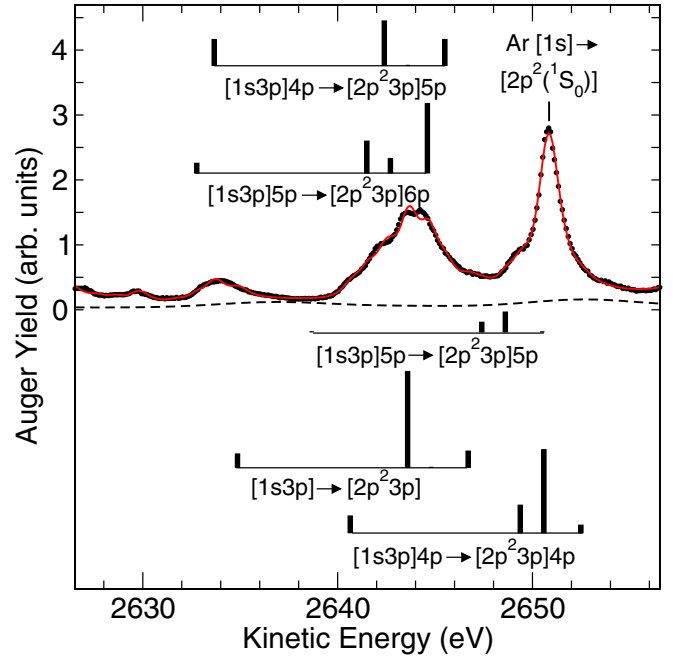

FIG. 7. Fit result of the Ar *KLL* Auger spectrum in the region of the Auger transitions of the Ar $[1s3p]n'l'$ photoelectron shake satellites to the $[2p^2(^1S_0, {}^1D_2)]$ double core hole; this spectrum is recorded with a photon energy $h\nu = 3400$ eV. The red solid line through the data points represents the fit result and the black dashed line the background. The five vertical-bar diagrams indicate the energy positions and relative intensities of the observed Auger transitions.

is shown in Fig. 7. Further below we will discuss the Ar $[1s3(s, p)]n'l' \rightarrow [2p^2(^1D)]$ knock-down Auger transitions (type 3), which are shown in Fig. 8; they contribute by roughly 0.5% to the Auger decays of the shake-up satellites.

The spectrum shown in Fig. 7 is fitted with the same approach as the shake-transitions during the Auger decay (discussed above). The result of this fit approach is given by the red solid line through the data points, while the background is indicated by the black dashed line. As the main result of the fit analysis, five vertical-bar diagrams indicate the energy positions and intensities of the observed transitions.

To assign these transitions only, the Ar $[1s3p]4p$, $[1s3p]5p$, and $[1s3p]$ initial states are taken into account. The first two initial states are the most intense singly ionized satellite states, as can be seen in the photoelectron spectrum (see Fig. 2). The doubly ionized $[1s3p]$ initial state caused by shake-off transitions is characterized by the emission of two electrons and cannot be observed in the present single-channel measurements. However, theoretical and experimental studies suggest that the $[1s3p]$ shake-off state has $\cong 20\%$ of the intensity of the $[1s]$ main line [32,33], so it has to be taken into account. For the initial states Ar $[1s3p]4p$ and $[1s3p]5p$ spectator (type 4) and shake-up (type 5) Auger decays to the final states $[2p^23p]4p$, $[2p^23p]5p$, and $[2p^23p]6p$ are taken into account. The energy positions of the transitions are estimated based on the energy positions of the $[1s3p]n'p'$ initial states taken from Fig. 2 and the $[2p^23p]n''l''$ final states taken from Fig. 6. Finally, the energy position of the $[1s3p] \rightarrow [2p^23p]$ transition (type 6) is estimated based on the $Z + 1$ approxi-
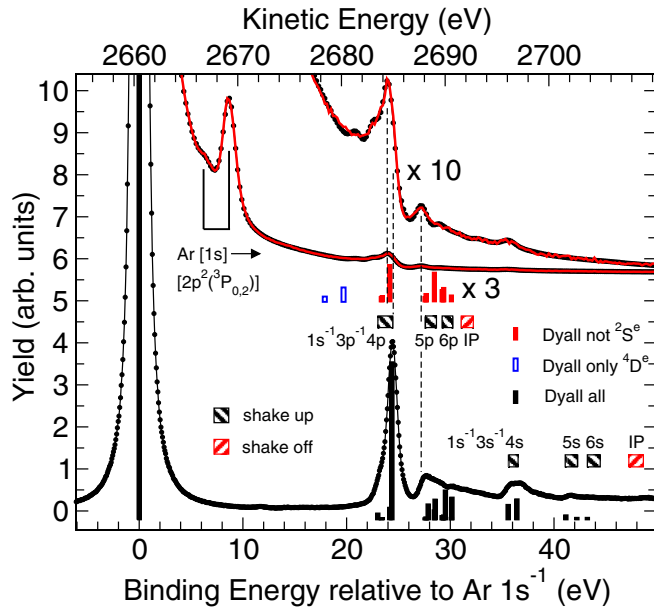
FIG. 8. The upper part shows the region of the $[1s3(s, p)]n'l' \to [2p^2(^1D_2)]$ transitions. The red solid line through the data points represents the fit result. The lower part indicates the photoelectron spectrum with the corresponding $[1s3(s, p)]n'l'$ shake satellites. The black filled vertical bars below the photoelectron spectrum indicate the intensities and energy positions of the shake satellites as calculated by Dyall [31]. The energy positions of the different $[1s3(s, p)]n'l'$ states as well as $[1s3(s, p)]$ double-ionization thresholds are indicated by the boxes above the spectrum. The red filled vertical bars below the Auger spectrum indicate the results of the calculations of Dyall, however limited to states with symmetries different from $^2S^e$ and intensity multiplied by a factor of 3. Finally, the blue hollow vertical bars at relative binding energies $\cong 19$ eV indicate the theoretical results of states with $^4D^e$ symmetry alone and the $[1s]$ main line aligned to the $[1s] \to [2p^2(^1S_0)]$ Auger transition. For more details, see the text.

mation for the core-hole state and the $Z + 2$ approximation for the final state, giving a kinetic energy of $\cong 19$ eV below the one of the corresponding $[1s] \to [2p^2]$ diagram line. In this way we obtain the assignment given below the various vertical-bar diagrams in Fig. 7.

Figure 4 exhibits also differences between the spectra recorded with the photon energies $h\nu = 3216$ and 3400 eV in the energy region from 2610 to 2630 eV. The spectrum measured at the latter photon energy shows generally higher intensities than the former. These differences are probably due to decays of higher-n' $[1s3p]n'p'$ or $[1s3s]n's'$ states as well as shake transitions like $[1s3p]4p \to [2p^23p]6p$, which are not taken into account in our analysis due to strong overlapping with the shakes during the Auger decay (type 2).

Finally, we discuss the Auger decay of the $[1s3(s, p)]n'l'$ shake-up states to the $[2p^2]$ configuration, i.e., transitions where the excited electron returns to its original shell (type 3). The relevant energy range is at kinetic energies above the $[1s] \to [2p^2]$ transitions and can be seen in the upper part of Fig. 8. For comparison, the lower part of the figure shows the $[1s3s]n's'$ and $[1s3p]n'p'$ satellite region of the

photoelectron spectrum with the $[1s]$ main line aligned to the $[1s] \to [2p^2(^1D)]$ diagram line in the Auger spectrum. The similarities in the photoelectron and the Auger spectra clearly support the assignment of the Auger structures to $[1s3(s, p)]n'l' \to [2p^2(^1D)]$ Auger transitions. Note that the background for the Auger spectrum is much more curved than in the photoelectron spectrum. This curvature is predominately due to the high-energy tail of the Lorentzian line shape of the $[1s] \to [2p^2(^1D)]$ transition and indicates that the intensity ratio of the $[1s3(s, p)]n'l' \to [2p^2]$ transitions and the $[1s] \to [2p^2(^1D)]$ diagram line in the Auger spectrum is much smaller than the intensity ratio of the $[1s3(s, p)]n'l'$ shake-up states and the $[1s]$ main photoelectron line.

Although the structures in the photoelectron and the Auger spectra are quite similar, a detailed comparison reveals interesting differences. First, we point out that we do not observe at $\cong 2674$ eV the $[2p^2(^1S)]$ counterpart to the $[1s3p]4p \to [2p^2(^1D)]$ transitions. One should expect to see this transition if one assumes the same intensity ratio for $[1s3p]4p \to [2p^2(^1S)]$ to $[1s3p]4p \to [2p^2(^1D)]$ transition as for the diagram lines $[1s] \to [2p^2(^1S)]$ and $[1s] \to [2p^2(^1D)]$ of about 1:10. Obviously, the intensity depends on the diagram line and the deexcitation of the excited electron is not a process of the valence shell alone. Second, the peak maxima in the Auger and the photoelectron spectrum differ in particular for the $[1s3p]4p$ and $[1s3p]5p$ shake-up satellites by about 600 meV, as indicated by the vertical dashed lines; this value is about one order of magnitude larger than the maximum expected error caused by aligning the two spectra to each other. This peak shift can be explained by a significant reduction of the intensity of the $^2S_{1/2}$ states (discussed below). Third, the exact spectral structure shows differences. For example, there is a clear minimum in the Auger spectrum at $\cong 2688.5$ eV which is missing in the photoelectron spectrum. Moreover, the line shapes of $[1s3p]4p$ and $[1s3s]4s$ clearly change. For the first peak the low-energy shoulder becomes more pronounced and for the second peak the high-energy component disappears completely. Since each spectral feature consists of different components, as can be seen by the black vertical bars below the photoelectron spectrum, we can conclude that the individual $[1s3(s, p)]n'l'$ shake-up states show different probabilities to decay to the $[2p^2]$ configuration.

In the following we discuss the reason for the individual decay probabilities for the $[1s3(s, p)]n'l'$ states. For this reason, the black filled vertical bars below the spectrum indicate the calculated intensities and energy positions for all Ar $[1s]$ shake satellites [31] and show generally good agreement between experiment and theory regarding both intensities and energy positions. In addition, the red filled vertical bars between the photoelectron and the Auger electron spectrum show the theoretical results for the states which have total symmetries different from $^2S_{1/2}$. Their intensities are multiplied by a factor of 3 as compared to the black filled vertical bars and they describe reasonably well the main spectral features of the Auger spectrum; this includes the peak shift to lower energy for both first peaks as discussed below. This result suggests that for the decay to the $[2p^2]$ configuration, shake-up states with a symmetry different from $^2S_{1/2}$ are preferred.

TABLE I. Summary of the absolute experimental kinetic energies $E_{\rm kin,expt}$ of the diagram lines (type 1) as well as the energies $E_{\rm rel,expt}$ relative to the Ar $[1s] \to [2p^2(^1D)]$ diagram line. For comparison, the relative kinetic energies $E_{\rm rel,theor}$ obtained by different theoretical studies are also given.

Configuration	$State$ $E_{\rm kin,expt}$ (eV)	$E_{\rm rel,expt}$			$E_{\rm rel,theor}$ (eV)			
		Present work	Ref. [5]	Ref. [6]	Ref. [5]	Ref. [6]	Ref. [4]	Ref. [1]
$[2p^2]$	$^3P_2$	8.66(1)	8.9	8.6	8.40	8.9	8.4	8
	$^3P_0$	6.51(5)		6.4	6.40	6.4	6.4	6
	$^1D_2$	0	0	0	0	0	0	0
	$^1S_0$	−9.66(1)	−9	−9.6	−8.10	−8.9	−8.0	−12
$[2s2p]$	$^3P_2$	−60.35(10)			−59.82	−60.2	−58.8	−57
	$^3P_1$	−61.75(20)	$\Big\}$−61.1	$\Big\}$−60.8	−61.22	−61.7	−60.1	−59
	$^3P_0$	−62.15(20)			−61.98	−62.5	−60.9	−58
	$^1P_1$	−84.89(1)	−84.7	−84.8	−85.09	−86.4	−84.2	−82
$[2s^2]$	$^1S_0$	−151.95(1)	−150.5	−151.6	−151.52	−153.6	−149.6	−142

From the observations we suggest as the most efficient decay mechanism to the $[2p^2]$ configuration a knock-down process, i.e., a *direct interaction* between the Auger electron leaving the $2p$ shell and the excited electron in the valence shell. In this way, the excited electron can exchange energy and momentum and jump back to its original $3s$ or $3p$ shell. In this context we point out that all calculated shake-up satellites in the photoelectron spectrum have *even* parity. The same holds for the final $[2p^2]$ configuration, so the outgoing Auger electron is only allowed to possess ϵs or ϵd character. Moreover, the Auger electron has to carry away the difference in angular momentum between the core-hole and the Auger final state. In the case of a $[2p^2(^1D)]$ final state and an ϵs Auger electron this is possible only for core-hole states with D-symmetry while for an ϵd Auger electron the symmetries S, P, D, F, and G are possible. However, for core-hole photoelectron satellites with S symmetry, the hole in the valence shell and the excited electron couple to zero. Since they also have to couple to an angular momentum of zero in the Auger final state due to the $3p^6$ valence shell, the valence shell cannot accept angular momentum from the outgoing Auger electron. As a result, the $[2p^2]$ configuration can be reached only via a shake-down process which is described by the overlap matrix elements $\langle 3s^{++}|ns^+\rangle$ and $\langle 3p^{++}|np^+\rangle$ with $++$, indicating the orbitals in the dicationic Auger final state and $+$ in the core-ionized state; these matrix elements are expected to be relatively small and explain the low intensities of the $^2S_{1/2}$ states in the Auger spectrum. In contrast, for the calculated $[1s]$ shake satellites with P or D symmetry the Auger electron can accept angular momentum, and as a consequence energy, more efficiently from the shaken valence electron, so the latter can jump back to its original shell.

For the Auger final state $[2p^2(^1S)]$ and ϵs Auger electron, the core-hole state has to be of S symmetry, and in the case of a ϵd Auger electron of D symmetry. Core-hole satellite states with P symmetry cannot decay in LS coupling to the $[2p^2(^1S)]$ state without violating either parity or angular momentum conservation; they are allowed only due to spin-orbit coupling and therefore are very weak. This situation is comparable with the $[2p^2(^3P)]$ diagram line, which is also very weak as compared to the $[2p^2(^1D)]$ diagram line for the same reason [10].

Since the core-hole states with S symmetry cannot exchange angular momentum with the Auger electron (discussed above), they are expected to be weak in the discussed type of Auger decay. This explains, together with the branching ratio for the decay to the $[2p^2(^1S)]$ and the $[2p^2(^1D)]$ state of about 1:10, why they are absent in the Auger spectrum. Contrary to this, core-hole satellites with D symmetry are allowed to exchange energy and angular momentum with the outgoing Auger electron so that they can decay to the $[2p^2(^1S)]$ Auger final state. Their expected energy positions based on the calculations of Dyall [31] and the splitting of the diagram lines (see Table I) are indicated with blue hollow bars below the Auger spectrum. The more intense line agrees quite well in energy with the spectral feature at $\cong$2681 eV, so we tentatively assign the latter feature to a $[1s3p]n'l'(D_{1/2}) \to [2p^2(^1S)]$ transition.

In summary, in this section we have presented the Auger transitions of the shake-up and shake-off states visible in the Ar $[1s]$ photoelectron spectrum. The transitions are assigned mainly based on the argument of energy positions. Finally, weak Ar $[1s3(s, p)]n'l' \to [2p^2(^1D)]$ transitions are observed and explained with the knock-down mechanism.

C. The Ar $[1s] \to [2s2p(^3P_{2,1,0})]$ diagram lines

Figure 9 shows the region of the Ar $[1s] \to [2s2p(^3P_{0,1,2})]$ diagram lines (type 1) measured subsequent to photoionization with a photon energy of $h\nu = 3400$ eV. This part of the spectrum also includes some Ar $[1s] \to [2p^2(^1S_0, {}^1D_2)3(s, p)]n''l''$ Auger shake-up transitions (see the dashed subspectrum). The dominating peak at 2600 eV caused by the Ar $[1s] \to [2s2p(^3P)]$ transition clearly exhibits an asymmetric line shape which is due to the observation of the splitting of the $[2s2p(^3P)]$ configuration into the final states $^3P_{0,1,2}$.

To obtain better insight into the splitting of the $[2s2p(^3P)]$ states, the spectrum was fitted with three broad Lorentzian lines of equal widths representing the three diagram lines (see the solid subspectrum). For these lines the intensity ratio was fixed to 1:3:5 according to the statistical weights; this approach is justified by the practically identical intensity ratios obtained by different calculations [2,5]. Contrary to
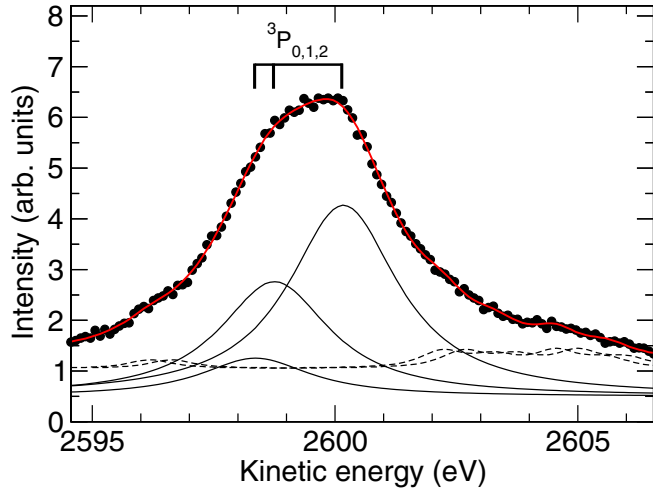
FIG. 9. Region of the Ar $[1s] \rightarrow [2s2p(^3P_{0,1,2})]$ diagram lines. The red solid line through the data points represents the fit result. The black solid subspectra indicate the contributions of the different diagram lines and are assigned by the vertical-bar diagram above the spectrum. The dashed subspectrum indicates the background including some Ar $[1s] \rightarrow [2p^2(^1S_0, {}^1D_2)3(s, p)]n''l''$ Auger shake-up transitions.

this, the energy positions were treated as free parameters. Moreover, a number of narrower lines representing Ar $[1s] \rightarrow [2p^2(^1S_0, {}^1D_2)3(s, p)]n''l''$ Auger shake-up transitions were included in the background (see the dashed subspectrum). The result of the fit is represented by the red solid line through the data points and yields the kinetic energy positions 2598.8(2), 2599.2(2), and 2600.6(1) eV for the transitions to the final states $^3P_0$, $^3P_1$, and $^3P_2$, respectively. The energy positions of the Ar $[1s] \rightarrow [2s2p(^3P_{0,1,2})]$ diagram lines relative to those of the Ar $[1s] \rightarrow [2p^2(^1D_2)]$ line are summarized in Table I, together with the values for the other diagram lines as obtained from the fit analyses presented above and below. The results of previous experimental and theoretical studies are also given, revealing in particular good agreement between the present results and the theoretical values of Ref. [5].

D. Lifetime broadening of Ar $[2s]$ or $[2s^2]$ containing states

In this section we investigate the lifetime broadenings of the SCH state Ar $[2s]$ as well as the DCH states $[2s^2(^1S_0)]$, $[2s2p(^1P_1)]$, and $[2s2p(^3P_{0,1,2})]$. The latter values are derived from the Auger spectrum by subtracting the well-known Ar $[1s]$ lifetime broadening [21], and are compared with the lifetime broadening of the SCH states Ar $[2s]$ and Ar $[2p]$. While the lifetime broadening of the Ar $[2p]$ core hole is well known from the literature [39], the values for the Ar $[2s]$ core hole given in the literature differ significantly from each other [40,41]. Because of this we derived an accurate value from an Ar $[2s]$ photoelectron spectrum recorded in the course of this study [see Fig. 10(a)]. We start by discussing the Ar $[2s]$ lifetime followed by the lifetimes of the DCH states. For convenience, the discussed experimental lifetime widths are summarized in Table II.

In a fit analysis of the Ar $[2s]$ spectrum, a lifetime broadening of $\Gamma_{[2s],\text{expt}} = 2.033(10)$ eV is derived, based on a
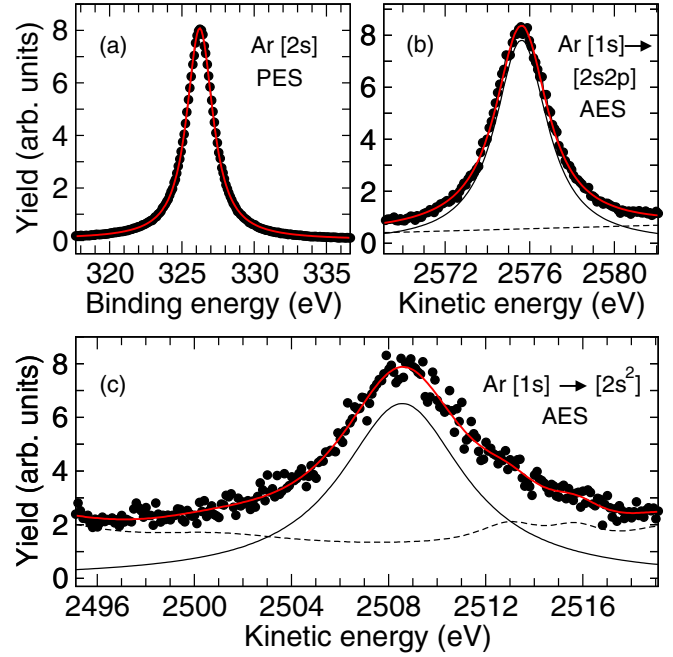

FIG. 10. The (a) Ar $[2s]$ photoelectron spectrum as well as (b) the Ar $[1s] \rightarrow [2s2p(^1P_1)]$ and (c) the Ar $[1s] \rightarrow [2s^2(^1S_0)]$ Auger transitions. The solid lines through the data points represent the fit result. In the case of (b) and (c) the solid subspectrum represents the respective diagram line and the dashed subspectrum the background partially including shake satellites.

Gaussian broadening of 0.545(10) eV representing the experimental resolution. The latter value was determined from an Ar $[2p]$ photoelectron spectrum using a lifetime broadening of $\Gamma_{[2p],\text{expt}} = 0.118(4)$ eV [39]. This value lies between the experimental value of $\Gamma_{[2s],\text{expt}} = 1.84(20)$ eV of Mehlhorn [40] and $\Gamma_{[2s],\text{expt}} = 2.25(5)$ eV of Glans *et al.* [41]. The present experimental lifetime broadening for the $[2s]$ core hole deviates considerably from the theoretical value of $\Gamma_{[2s],\text{theor}} = 1.63$ eV obtained by Krause and Oliver [42]. This deviation for the $[2s]$ hole is in contrast to the results of Krause and Oliver for the Ar $[1s]$ hole ($\Gamma_{[1s],\text{expt}} = 0.655$ eV [21] and $\Gamma_{[1s],\text{theor}} = 0.680$ eV) and Ar $[2p]$ hole [$\Gamma_{[2p],\text{expt}} = 0.118(4)$ eV [39]

TABLE II. Summary of the experimental argon SCH and DCH lifetime widths Γ_{expt}. For comparison with the DCH lifetimes, sums of the corresponding SCH lifetimes Γ_{sum} are also given. For the sum values, an Ar $[2s]$ lifetime width of $\Gamma = 2.033(10)$ eV is used.

Core hole state	Γ_{expt} (eV)	Γ_{sum} (eV)
$[2p]$	0.118(4)[a]	
$[2s]$	2.033(10), 1.84(20),[b] 2.25(5)[c]	
$[1s]$	0.665[d]	
$[2p^2]$	0.323(15)[e]	0.236(8)
$[2s2p(^3P)]$	2.02(8)	
$[2s2p(^1P)]$	2.18(2)	
$[2s2p]$[f]	2.17(2)	2.151(14)
$[2s^2]$	5.49(44)	4.066(20)

[a]Reference [39]; [b]Reference [40]; [c]Reference [41]; [d]Reference [21]; [e]Reference [22]; [f]Weighted average.

and $\Gamma_{[2p],\text{theor}} = 0.127$ meV], where good agreement between experiment and theory was found. Better agreement of the present experimental result of $\Gamma_{[2s],\text{expt}} = 2.033(10)$ is found with the theoretical results of Glans *et al.* of $\Gamma_{[2s],\text{theor}} = 1.85$ eV [41].

In a fit analysis the Lorentzian width of the Ar $[1s] \rightarrow [2s^2(^1S_0)]$ diagram line shown in Fig. 10(c) turns out to be $\Gamma = 6.15(44)$ eV. This value still contains the Ar $[1s]$ lifetime, so we obtain $\Gamma_{[2s^2],\text{expt}} = 5.49(44)$ eV for the $[2s^2(^1S_0)]$ DCH state. This results in a ratio of 2.70(22) for the lifetimes of the $[2s^2]$ and the $[2s^1]$ states, in good agreement with the ratios of 2.76(25) for the Ar $[2p]$ core-hole states [22] and 2.9(1) for the Ne $[1s]$ core-hole states [23], and confirms for shallow core levels that the DCH lifetime is significantly shorter than half the SCH lifetime. This observation is a result of the fact that the orbitals energetically above the vacant orbitals experience a higher charge due to the missing electrons, so they shrink and have better overlap with the core hole; this results in a significant increase of the Auger rates. Note that for deeper core holes the ratio is expected to converge to 2 [23]. This is in agreement with the finding of 1.88(25) for the I $(3d_{5/2})$ level in CH_3I [43].

In the next step we investigate the mixed $[2s2p]$ DCH states, which exhibit a different behavior. The Ar $[1s] \rightarrow [2s2p(^3P_{0,1,2})]$ and Ar $[1s] \rightarrow [2s2p(^1P_1)]$ diagram lines including the fit results are shown in Figs. 9 and 10(b), respectively. The obtained Lorentzian widths are $\Gamma = 2.68(8)$ eV for the Ar $[1s] \rightarrow [2s2p(^3P_{0,1,2})]$ transition and $\Gamma = 2.84(2)$ eV for the Ar $[1s] \rightarrow [2s2p(^1P_1)]$ transition. Although the error bars do not allow us to derive different lifetimes for the $[2s2p(^1P_1)]$ and $[2s2p(^3P_{0,1,2})]$ states, we would like to point out that for the corresponding states of Br in HBr such differences have been pinpointed experimentally and theoretically [44]. However, since in the present case the differences are very small and do not influence the discussion, we assume in the following identical lifetimes for the $[2s2p(^3P_{0,1,2})]$ and $[2s2p(^1P_1)]$ core-hole states and obtain a weighted average value $\Gamma = 2.83(2)$ eV. After subtraction of the Ar $[1s]$ lifetime broadening, a value of $\Gamma_{[2s2p],\text{expt}} = 2.17(2)$ eV is obtained. This lifetime broadening agrees well with the sum of the $[2s]$ and the $[2p]$ core hole of 2.151(14) eV.

This behavior can be understood based on the dominating decay channel of the Ar $[2s]$ core hole, namely, the $[2s] \rightarrow [2p3l]$ Coster-Kronig Auger decay, which explains the short lifetime of the $2s$ vacancy. As a result of the additional vacancy in the $2p$ shell, the numbers of Coster-Kronig Auger decay channels is statistically reduced by a factor of $\frac{5}{6}$. By taking this factor into account one obtains a lifetime broadening of $\frac{5}{6}\Gamma_{[2s],\text{expt}} + \Gamma_{[2p],\text{expt}} = 1.810$ eV, i.e., a value which is too small, so the difference between this value and the experimental result of $\Gamma_{[2s2p],\text{expt}} = 2.17(2)$ eV has to be explained by the contraction of the outermost orbitals. A similar effect has been observed for the Ar $[1s2p]$ double-core-hole states [24].

In summary, the results on $[2s2p]$ reveal that competing processes influence the lifetime on mixed DCH states, namely, the reduction of Auger channels and the increase of the rates of each channel, due to a contraction of the orbitals involved.

V. CONCLUSION

State-of-the-art argon *KLL* Auger spectra were presented together with an Ar $1s^{-1}$ photoelectron spectrum. The latter spectrum allowed us to investigate in detail the Ar $[1s3(s, p)]n'l'$ photoelectron satellite structures, whose non-radiative decay also contributes to the Auger spectrum. A complete assignment of all satellite structures was performed. Furthermore, six types of different decay pathways were analyzed in great detail. The spectra were measured at photon energies of $h\nu = 3216$ and 3400 eV, i.e., below and above the Ar $[1s3(s, p)]n'l'$ photoelectron satellites. This allowed us to distinguish between the shake transitions during the Auger decay (type 2) and the Auger transitions of the photoelectron satellites (types 4–6), since the latter are only present in the spectrum measured at 3400 eV. While the decays of the photoelectron satellites were assigned in previous studies of the Ar *KLL* Auger spectrum [5,6], the shake transitions during the Auger decay were assigned before only for H_2S [20], so the present results support that these transitions are a general effect. Moreover, we found that the shakes during the Auger transitions contribute 4.8(1.0)% to the spectrum of the Ar $[1s] \rightarrow [2l^2]$ decays.

For the decay of the photoelectron satellites shake-up and spectator transitions were observed. In addition, Ar $[1s3(s, p)]n'l' \rightarrow [2p^2(^1D_2)]$ transitions (type 3), i.e., transitions where the $n'l'$ electron fills the $[3l]$ vacancy, were observed; these we mainly assigned to knock-down transitions with an exchange of angular momentum between the excited and the Auger electron.

For the $[1s] \rightarrow [2s2p(^3P_J)]$ transition the different components with $J = 2, 1, 0$ were resolved. Moreover, the lifetime broadenings of the Ar $[2s]$ SCH state and the $[2s^2]$ and $[2s2p]$ DCH states were determined, confirming previously observed trends for DCH states.

[1] D. A. Shirley, Theory of *KLL* Auger energies including static relaxation, Phys. Rev. A **7**, 1520 (1973).

[2] M. H. Chen and B. Crasemann, *K-LL* Auger transition probabilities for elements with low and intermediate atomic numbers, Phys. Rev. A **8**, 7 (1973).

[3] M. O. Krause, Argon *KLL* Auger Spectrum: A Test of Theory, Phys. Rev. Lett. **34**, 633 (1975).

[4] F. P. Larkins, Semi-empirical Auger electron energies. I. General method and *K-LL* line energies, J. Phys. B **9**, 47 (1976).

[5] J. Vayrynen, R. N. Sodhi, and R. G. Cavell, Energies and intensities of the *KLL* Auger spectra of SiH_4, PH_3, HCl, and Ar, J. Chem. Phys. **79**, 5329 (1983).

[6] L. Asplund, P. Kelfve, B. Blomster, H. Siegbahn, and K. Siegbahn, Argon *KLL* and *KLM* Auger electron spectra, Phys. Scr. **16**, 268 (1977).

[7] T. D. Thomas, Transition from Adiabatic to Sudden Excitation of Core Electrons Phys. Rev. Lett. **52**, 417 (1984).

[8] S. H. Southworth, T. LeBrun, Y. Azuma, and K. G. Dyall, Argon KM photoelectron satellites J. Electron Spectrosc. Relat. Phenom. **94**, 33 (1998).

[9] O. Travnikova, M. Patanen, J. Söderström, A. Lindblad, J. J. Kas, F. D. Vila, D. Céolin, T. Marchenko, G. Goldsztejn, R. Guillemin, L. Journel, T. X. Carroll, K. J. Børve, P. Decleva, J. J. Rehr, N. Mårtensson, M. Simon, S. Svensson, and L. J. Sæthre, Energy-dependent relative cross sections in carbon 1*s* photoionization: Separation of direct shake and inelastic scattering effects in single molecules, J. Phys. Chem. A **123**, 7619 (2019).

[10] V. Schmidt, *Electron Spectrometry of Atoms using Synchrotron Radiation* (Cambridge University Press, Cambridge, 1997).

[11] K. Faegri and O. Keski-Rahkonen, Sulphur *KLL* Auger spectra of gaseous sulphur compounds, J. Electron Spectrosc. Relat. Phenom. **11**, 275 (1976).

[12] L. Asplund, P. Kelfve, B. Blomster, H. Siegbahn, K. Siegbahn, R. L. Lozes, and U. I. Wahlgren, Molecular Auger electron spectra of second row elements. Sulfur compounds, Phys. Scr. **16**, 273 (1977).

[13] P. A. Heimann, D. W. Lindle, T. A. Ferrett, S. H. Liu, L. J. Medhurst, M. N. Piancastelli, D. A. Shirley, U. Becker, H. G. Kerkhoff, B. Langer, D. Szostak, and R. Wehlitz, Shake-off on inner-shell resonances of Ar, Kr and Xe, J. Phys. B **20**, 5005 (1987).

[14] H. Aksela, S. Aksela, H. Pulkkinen, G. M. Bancroft, and K. H. Tan, Anomalously strong shake-up processes in Auger decay of the resonantly excited $2p^5 3s^2 3p^6 nl$ states of Ar, Phys. Rev. A **37**, 1798(R) (1988).

[15] S. Sundin, F. Kh. Gel'mukhanov, S. J. Osborne, O. Björneholm, A. Ausmees, A. Kikas, S. L. Sorensen, A. Naves de Brito, R. R. T. Marinho, S. Svensson, and H. Ågren, Auger decay of core-excited higher Rydberg states of carbon monoxide, J. Phys. B **30**, 4267 (1997).

[16] R. Püttner, Y. F. Hu, G. M. Bancroft, A. Kivimäki, M. Jurvansuu, H. Aksela, and S. Aksela, Strong nonmonopole shake transitions in the Br $3d^{-1} np\pi$ ($n = 6$–9) resonant Auger spectra of HBr, Phys. Rev. A **77**, 032705 (2008).

[17] G. Goldsztejn, R. Püttner, L. Journel, R. Guillemin, O. Travnikova, R. K. Kushawaha, B. Cunha de Miranda, I. Ismail, D. Céolin, M. N. Piancastelli, M. Simon, and T. Marchenko, Electronic-state-lifetime interference in the hard-x-ray regime: Argon as a showcase Phys. Rev. A **95**, 012509 (2017).

[18] T. Kantia, L. Partanen, S. Aksela, and H. Aksela, High resolution KLL Auger spectra of free sodium and magnesium atoms, J. Electron Spectrosc. Relat. Phenom. **180**, 58 (2010).

[19] T. Kantia, S. Aksela, P. Turunen, L. Partanen, and H. Aksela, KLL Auger decay of atomic silicon, J. Phys. B **43**, 205002 (2010).

[20] R. Püttner, D. Céolin, R. Guillemin, R. K. Kushawaha, T. Marchenko, L. Journel, M. N. Piancastelli, and M. Simon, Detailed analysis of shake structures in the *KLL* Auger spectrum of H_2S, Phys. Rev. A **93**, 042501 (2016).

[21] D. Céolin, J. M. Ablett, D. Prieur, T. Moreno, J. P. Rueff, T. Marchenko, L. Journel, R. Guillemin, B. Pilette, T. Marin, and M. Simon, Hard x-ray photoelectron spectroscopy on the GALAXIES beamline at the SOLEIL synchrotron, J. Electron Spectrosc. Relat. Phenom. **190**, 188 (2013).

[22] M. Žitnik, R. Püttner, G. Goldsztejn, K. Bučar, M. Kavčič, A. Mihelič, T. Marchenko, R. Guillemin, L. Journel, O. Travnikova, D. Céolin, M. N. Piancastelli, and M. Simon, Two-to-one Auger decay of a double *L* vacancy in argon, Phys. Rev. A **93**, 021401(R) (2016).

[23] G. Goldsztejn, T. Marchenko, R. Püttner, L. Journel, R. Guillemin, S. Carniato, P. Selles, O. Travnikova, D. Céolin, A. F. Lago, R. Feifel, P. Lablanquie, M. N. Piancastelli, F. Penent, and M. Simon, Double-Core-Hole States in Neon: Lifetime, Post-Collision Interaction, and Spectral Assignment, Phys. Rev. Lett. **117**, 133001 (2016).

[24] R. Püttner, G. Goldsztejn, D. Céolin, J.-P. Rueff, T. Moreno, R. K. Kushawaha, T. Marchenko, R. Guillemin, L. Journel, D. W. Lindle, M. N. Piancastelli, and M. Simon, Direct Observation of Double-Core-Hole Shake-Up States in Photoemission, Phys. Rev. Lett. **114**, 093001 (2015).

[25] M. Simon, R. Püttner, T. Marchenko, R. Guillemin, R. K. Kushawaha, L. Journel, G. Goldsztejn, M. N. Piancastelli, J. M. Ablett, J.-P. Rueff, and D. Céolin, Atomic Auger Doppler effects upon emission of fast photoelectrons, Nat. Commun. **5**, 4069 (2014).

[26] M. Breinig, M. H. Chen, G. E. Ice, F. Parente, B. Crasemann, and G. S. Brown, Atomic inner-shell level energies determined by absorption spectrometry with synchrotron radiation, Phys. Rev. A **22**, 520 (1980).

[27] M. Alagia, R. Richter, S. Stranges, M. Agåker, M. Ström, J. Söderström, C. Såthe, R. Feifel, S. Sorensen, A. De Fanis, K. Ueda, R. Fink, and J.-E. Rubensson, Core level ionization dynamics in small molecules studied by x-ray-emission threshold-electron coincidence spectroscopy, Phys. Rev. A **71**, 012506 (2005).

[28] P. Jönsson, X. He, C. Froese Fischer, and I. P. Grant, The grasp2K relativistic atomic structure package, Comput. Phys. Commun. **177**, 597 (2007).

[29] S. Fritzsche, The RATIP program for relativistic calculations of atomic transition, ionization and recombination properties, Comput. Phys. Commun. **183**, 1525 (2012).

[30] M. Hrast, A. Mihelič, K. Bučar, and M. Žitnik, Auger decay of the 2*p* vacancy in chlorine, Phys. Rev. A **100**, 023408 (2019).

[31] K. G. Dyall, Shake theory predictions of excited-state populations following 1s ionisation in argon, J. Phys. B **16**, 3137 (1983).

[32] T. A. Carlson and C. W. Nestor, Jr., Calculation of electron shake-off probabilities as the result of x-ray photoionization of the rare gases, Phys. Rev. A **8**, 2887 (1973).

[33] J.-Cl. Dousse and J. Hoszowska, *L*- and *M*-shell-electron shake processes following 1*s* photoionization in argon and krypton, Phys. Rev. A **56**, 4517 (1997).

[34] NIST Atomic Level Database, version 5, http://www.nist.gov/pml/data/asd.cfm.

[35] N. Mårtensson and A. Nilsson, in *Applications of Synchrotron Radiation: High-Resolution Studies of Molecules and Molecular Adsorbates on Surfaces*, edited by W. Eberhardt, Springer Series in Surface Sciences (Springer, Berlin, 1995), Vol. 35, pp. 65–126.

[36] S. Svensson, B. Eriksson, N. Mårtensson, G. Wendin, and U. Gelius, Electron shake-up and correlation satellites and continuum shake-off distributions in x-ray photoelectron spectra of the rare gas atoms, J. Electron Spectrosc. Relat. Phenom. **47**, 327 (1988).

[37] R. Guillemin, S. Sheinerman, R. Püttner, T. Marchenko, G. Goldsztejn, L. Journel, R. K. Kushawaha, D. Céolin, M. N. Piancastelli, and M. Simon, Postcollision interaction effects in *KLL* Auger spectra following argon 1*s* photoionization, Phys. Rev. A **92**, 012503 (2015).

[38] R. Huster, W. Sandner, and W. Mehlhorn, Post-collision interaction in inner-shell ionisation by electron impact: Energy shift of *KLL* Auger electrons of Ne and Ar, J. Phys. B **20**, L287 (1986).

[39] M. Jurvansuu, A. Kivimäki, and S. Aksela, Inherent lifetime widths of Ar $2p^{-1}$, Kr $3d^{-1}$, Xe $3d^{-1}$, and Xe $4d^{-1}$ states, Phys. Rev. A **64**, 012502 (2001).

[40] W. Mehlhorn, Das Coster-Kronig- und Auger-spektrum der L_1-schale von argon, Z. Phys. **208**, 1 (1968).

[41] P. Glans, R. E. LaVilla, M. Ohno, S. Svensson, G. Bray, N. Wassdahl, and J. Nordgren, Determination of the lifetime width of the argon L_1-hole state, Phys. Rev. A **47**, 1539 (1993).

[42] M. O. Krause, and J. H. Oliver, Natural widths of atomic *K* and *L* levels, $K\alpha$ x-ray lines and several *KLL* Auger lines, J. Phys. Chem. Ref. Data **8**, 329 (1979).

[43] T. Marchenko, G. Goldsztejn, K. Jänkälä, O. Travnikova, L. Journel, R. Guillemin, N. Sisourat, D. Céolin, M. Žitnik, M. Kavčič, K. Bučar, A. Mihelič, B. Cunha de Miranda, I. Ismail, A. F. Lago, F. Gel'mukhanov, R. Püttner, M. N. Piancastelli, and M. Simon, Potential Energy Surface Reconstruction and Lifetime Determination of Molecular Double-Core-Hole States in the Hard X-Ray Regime, Phys. Rev. Lett. **119**, 133001 (2017).

[44] N. Boudjemia, K. Jänkälä, R. Püttner, T. Marchenko, O. Travnikova, R. Guillemin, L. Journel, I. Ismail, D. Koulentianos, S. Kosugi, Y. Azuma, M. Patanen, M. Huttula, D. Céolin, M. N. Piancastelli, and M. Simon, Electron spectroscopy and dynamics of HBr around the Br $1s^{-1}$ threshold, Phys. Chem. Chem. Phys. (2020), doi: 10.1039/D0CP04787B.